THE JOURNAL OF PHYSICAL CHEMISTRY C
A JOURNAL OF THE AMERICAN CHEMICAL SOCIETY

pubs.acs.org/JPCC

Article

Giant Negative Linear Compressibility, Isosymmetric Phase Transition, and Breathing Effect in a 3D Covalent Organic Framework

Mustafa Erkartal*

Cite This: J. Phys. Chem. C 2024, 128, 588−596

Read Online

ACCESS | Metrics & More | Article Recommendations | Supporting Information

ABSTRACT: A set of remarkable piezo-mechanical properties, including isosymmetric phase transition, negative linear compressibility (NLC), and a breathing effect in a three-dimensional covalent organic framework (NPN-3), was uncovered using density functional theory. The pressure-induced first-order phase transition observed between 0.9 and 1 GPa is isosymmetric and irreversible. NPN-3 shows giant NLC along the *c*-axis (K_c = 42.04 TPa^{-1}) prior to the phase transition. The high-density NPN-3-hd obtained as a result of the phase transition shows an exciting phase transition from a closed pore to an open pore under hydrostatic tensile pressure, similar to the breathing effect. These extraordinary piezo-mechanical attributes within NPN-3 can be attributed to the diamondoid (**dia**) topology, which is commonly found within flexible MOFs and COFs. Additionally, the remarkable adaptability of the tetraphenyl adamantane monomer to distinct conformations under pressure can be seen in these properties. These findings underscore the potential utility of COFs as materials for piezo-mechanical sensors and serve as a source of inspiration for further exploration into the intricate mechanical behaviors of COFs.

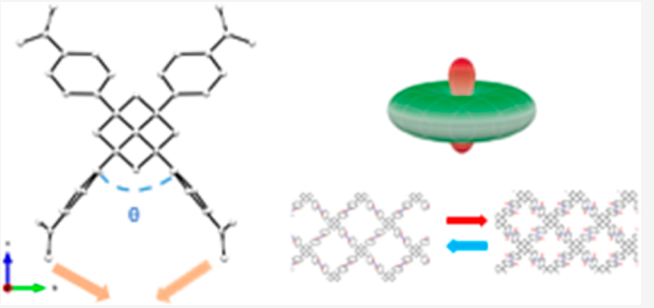

INTRODUCTION

Flexible porous crystals have emerged as highly intriguing materials in the field of materials science, capturing significant interest due to their unique combination of structural flexibility and porosity.[1−3] In contrast to rigid porous crystals, these crystals possess flexible pores that can undergo reversible phase transformations in response to external stimuli including host−guest interactions, temperature, and pressure. This diverse class of materials encompasses a wide range of structures, such as metal−organic frameworks (MOFs),[4,5] covalent organic frameworks (COFs),[6,7] zeolites,[8,9] and porous organic polymers.[10,11] Their inherent flexibility allows for significant changes in their crystal structures, leading to a wide range of functional properties, including tunable porosity,[12,13] selective adsorption,[14,15] guest molecule release,[16,17] and stimulus-responsive behavior.[18,19]

The exceptional flexibility of these porous crystals arises from their unique architectures, which consist of rigid building blocks interconnected by flexible linkers. The presence of these flexible elements enables the materials to undergo structural transformations, often referred to as "breathing" or "gate-opening" effects.[20] In addition to the inherent degrees of freedom of the building blocks, the structural motifs present in flexible crystals contribute to their ability to exhibit anomalous mechanical properties, including negative linear compressibility (NLC)[21,22] and zero linear compressibility (ZLC).[23−25] NLC, defined as an unusual property wherein a substance expands along a specific direction when isotropically compressed,[26] has been observed in several MOFs including the MIL-53 family,[27,28] [InH-$(BDC)_2$],[29] ZAG-4,[30] MFM-133 (Hf),[31] MCF-34,[32] and several more.[33−36] The underlying mechanisms of NLC in MOFs have been attributed to the wine-rack/β-quartz structural motif and strut-hinges mechanism.

While the high-pressure behavior and mechanical properties of MOFs have been extensively investigated in numerous studies, the same level of understanding is lacking for COFs. Limited work has been conducted on COFs with few theoretical predictions[7,37−39] and only a few experimental investigations reported so far.[6,40] One of the main challenges in studying the mechanical properties of COFs is the difficulty in synthesizing them as single crystals. COF synthesis often results in polycrystalline or amorphous materials, which hinders the application of experimental techniques,[41] such as diamond anvil cells (DACs), to determine pressure-dependent mechanical properties. In addition to experimental difficulties, computa-

Received: October 20, 2023
Revised: December 3, 2023
Accepted: December 12, 2023
Published: December 26, 2023

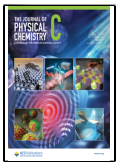

https://doi.org/10.1021/acs.jpcc.3c06949
J. Phys. Chem. C 2024, 128, 588−596

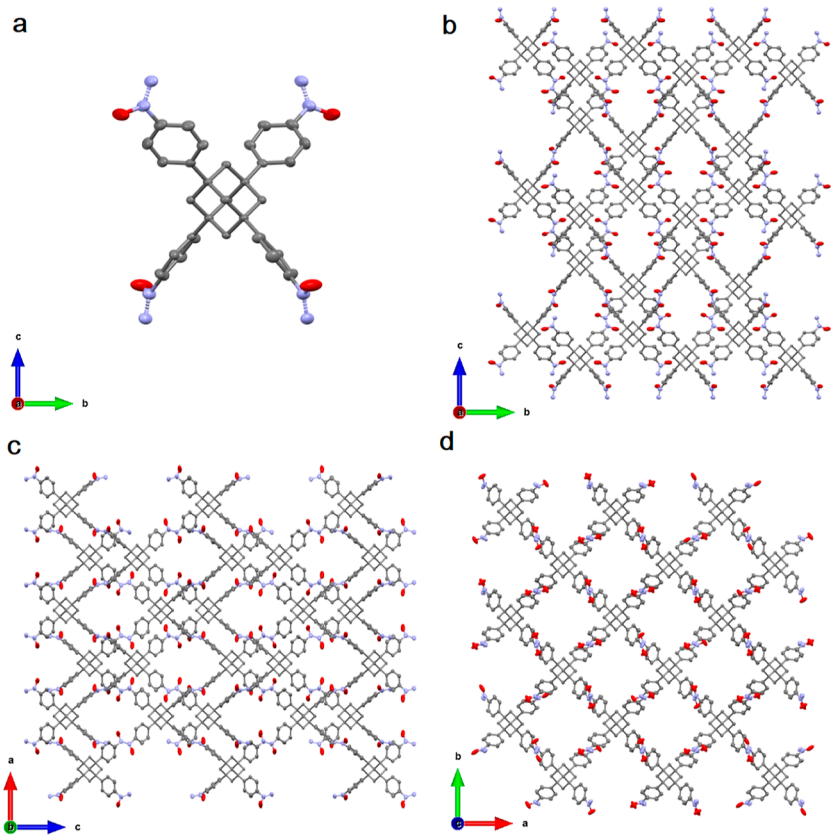

Figure 1. (a) Molecular structure of monomer 1,3,5,7-tetrakis(4-nitrosophenyl)adamantane. View of the extended structure of NPN-3 along the (b) *a*-axis, (c) *b*-axis, and (d) *c*-axis. The structure has sixfold interpenetration and open channels along the *c*-axis.

tional studies of COFs face their own set of challenges. Structures modeled based on powder X-ray diffraction (PXRD) data often suffer from uncertainties in atomic positions, geometric parameters, and guest arrangements within the pores. The presence of interpenetrated frameworks and disorder further complicates computational investigations.

In this study, the piezo-mechanical behavior of a 3D COF, named NPN-3, was investigated using density functional theory (DFT), taking advantage of recent advancements in growing 3D COFs as single crystals and accurately determining their atomistic structures. For this purpose, the unit cell obtained from the single crystal was optimized, followed by the application of hydrostatic pressure to the structure in both tensile and compressive regions. The obtained results are analyzed by considering symmetric modifications, linear compressibility, and pressure-dependent structural motifs.

COMPUTATIONAL DETAILS

All first-principles calculations were conducted using Quantum Espresso (QE) package,[42] which employs a plane wave-based DFT. The electron−ion interactions were described using projector augmented wave (PAW) potential,[43] chosen for its ability to effectively simulate high-pressure conditions.[7,23,44,45] The exchange−correlation potential was treated with the generalized gradient approximation (GGA) and the Perdew−Burke−Ernzerhof (PBE) parameterization.[46] To account for dispersive interactions, we introduced Grimme's semiempirical potential (DFT-D2) within the GGA framework.[47] Full structural optimization was carried out using the Broyden−Fletcher−Goldfarb−Shanno (BFGS) minimization scheme,[48] setting convergence criteria at 10^{-3} eV/Å for residual forces and 10^{-6} eV for energy differences between consecutive optimization steps. The Brillouin zone integration was executed using a Monkhorst−Pack[49] *k*-space mesh of dimensions 2 × 2 × 4. The kinetic energy and charge density cutoff values were specified as 80 and 600 Ry, respectively. During the optimization process, both atomic positions and unit cell parameters were relaxed, utilizing the experimentally derived unit cell of NPN-3 as the starting configuration. Investigation of the pressure-dependent elastic constants involved applying strain to the lattice and allowing the relaxation of internal degrees of freedom, with the elastic constants determined from changes in the stress tensor resulting from the applied strain. These computational tasks were conducted with the thermo_pw package.[50] For a comprehensive study of the framework's response to hydrostatic pressure, a series of successive enthalpy minimization calculations at different pressure values were conducted, commencing from the optimized structure. This allowed us to monitor the evolution of the unit parameters as a function of pressure. For visualization purposes, we employed the Mercury program, symmetry analysis of high-pressure phases was carried out using the PLATON code,[51] mechanical properties were derived using the ELATE code,[52] and postprocessing of Quantum Espresso data was performed with the Atomsk software.[53]

RESULTS AND DISCUSSION

NPN-3, a nitroso polymer network, represents a significant breakthrough as the one of first 3D COFs with a fully characterized structure using single-crystal XRD (SXRD).[54] The framework of NPN-3 consists of trans-azo-dioxide linkages and is synthesized through polymerization from 1,3,5,7-

https://doi.org/10.1021/acs.jpcc.3c06949
J. Phys. Chem. C 2024, 128, 588−596

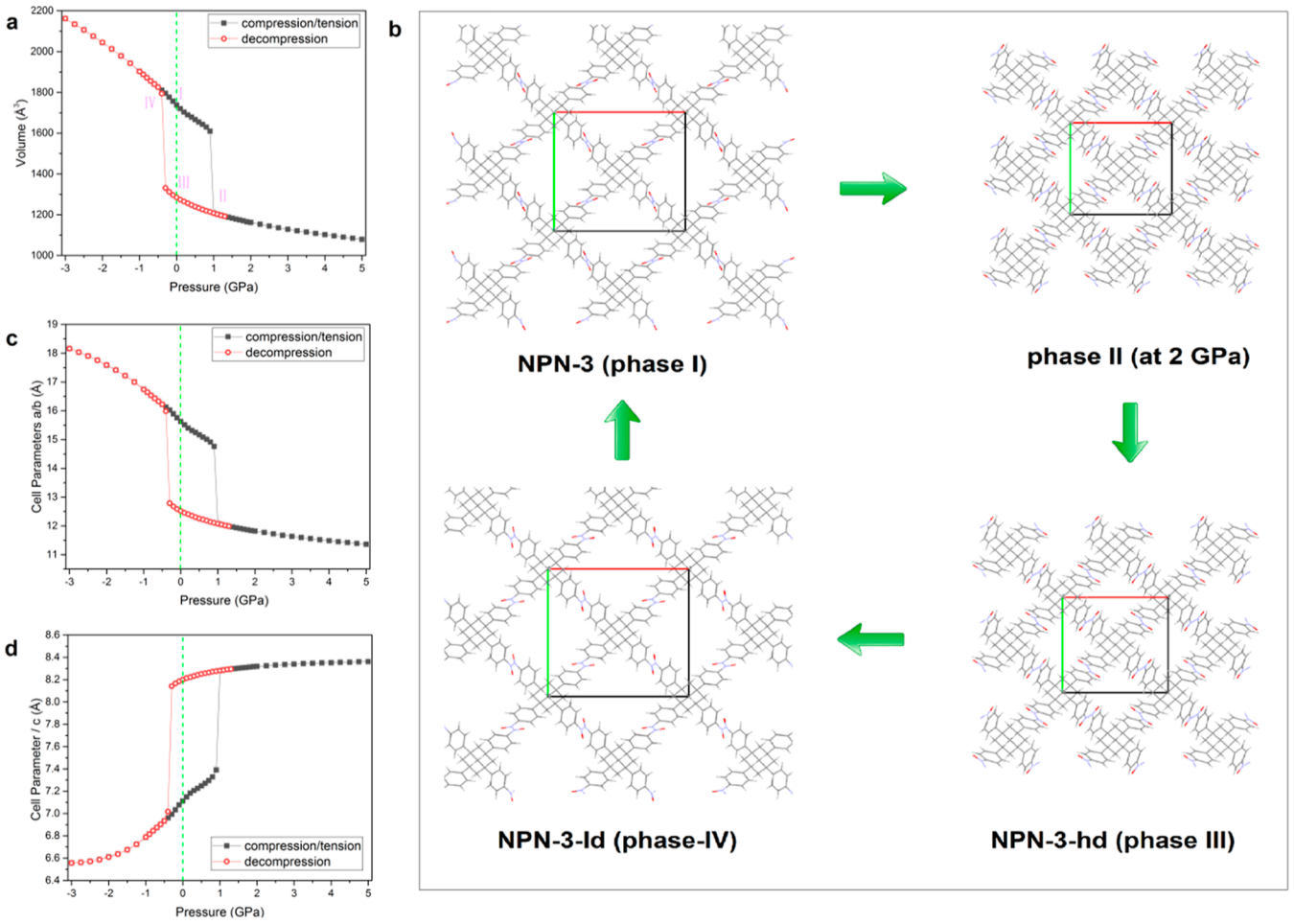

Figure 2. (a) Evolution of the NPN-3 unit cell under hydrostatic pressure in the compression and tensile regimes. (b) Depiction of the changes of NPN-3 in these pressure regimes along the *c*-axis on the extended crystal structure. (c,d) Evolution of the unit cell parameters under hydrostatic pressure.

tetrakis(4-nitrosophenyl)adamantane monomer (Figure 1a), resulting in the formation of a diamondoid (**dia**) network (Figure 1b,c). This diamondoid network exhibits an open structure that enables sixfold interpenetration along the *c*-axis (Figure 1d). NPN-3 is packed under the tetragonal crystal system with the $P4_2/n$ space group.

First, to relax NPN-3, the experimentally reported low temperature (100 K) structure was subjected to variable-cell optimization, involving the optimization of both atomic positions and unit cell parameters. Previous studies have demonstrated the reliability of in silico methods in simulating the effects of hydrostatic pressure at low temperatures,[44,55,56] providing results that closely match experimental observations. The calculated 0 K lattice parameters of 15.63 and 7.11 Å are in excellent agreement with experimental values[54] of 15.77 and 7.07 Å, as well as the relaxed structure has the same space group as the initial system. Then, the relaxed structure was subjected to hydrostatic pressure in both tensile (up to −3 GPa) and compression (up to 5 GPa) regions, and full structural relaxation was performed under these pressurized conditions.

Figure 2a shows the evolution of the unit cell volume of NPN-3 in the compression and tension regions. In the tensile region, no phase transitions, structural failures, or bond breakages were observed. The volume of NPN-3 increases gradually in this region, reaching a maximum of approximately 25%. In the compression regime, a linear decrease in the structure volume of about 7% was observed up to 0.9 GPa. Between 0.9 and 1 GPa, a first-order phase transition occurred, accompanied by a 25% volume decrease. This denser structure, termed phase II or NPN-3-hd, has the same space symmetry as NPN-3, indicating an isosymmetric phase transition. No further phase transitions were observed in the compression region between 1 and 5 GPa, but the volume of the framework decreased by approximately 11%. Upon pressure release, the structure recovered only around 6% of its volume, indicating the irreversibility of the phase transition. Notably, in the tensile region, interesting behavior was observed for NPN-3-hd. Between 0.3 and 0.4 GPa, the volume of the structure increases rapidly, leading to a phase transition. Similar to all other structures obtained in this research, this structure also has $P4_2/n$ symmetry, indicating a first-order isosymmetric phase transition. Following the phase transition in the tensile region, phase-IV adopted the same P−V pattern as NPN-3.

Clearly, NPN-3 exhibits a breathing effect similar to MOFs,[57] with open (op) and closed pore (cp) forms observed in the compression and tensile regions (Figure 2b). Unlike MOFs, the op-to-cp phase transition in NPN-3 during compression is an isosymmetric phase transition with an unchanged crystalline space group. This breathing effect is also evident in the solvent-accessible volume (SAV), which is relevant for gas storage and guest encapsulation. NPN-3 has a porosity of approximately 34%, while phase II and phase III (NPN-3-hd) have values of 3.2

https://doi.org/10.1021/acs.jpcc.3c06949
J. Phys. Chem. C 2024, 128, 588−596

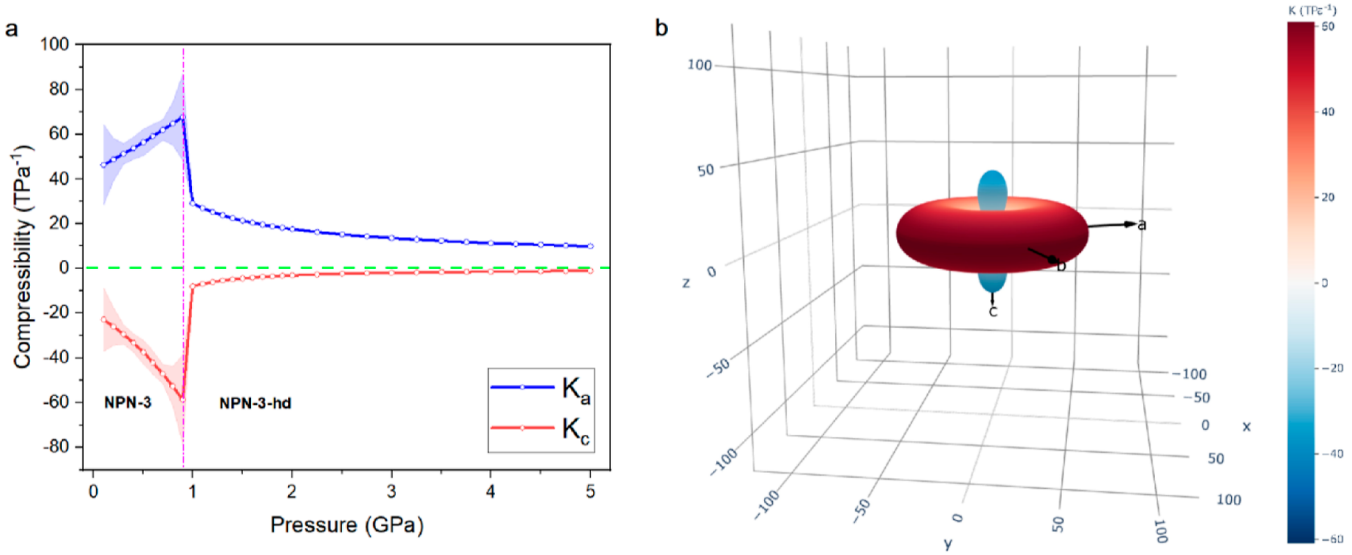

Figure 3. (a) Lattice compressibilities of NPN-3 and NPN-3-hd as a function of pressure. (b) Compressibility indicatrix of the ambient phase of NPN-3.

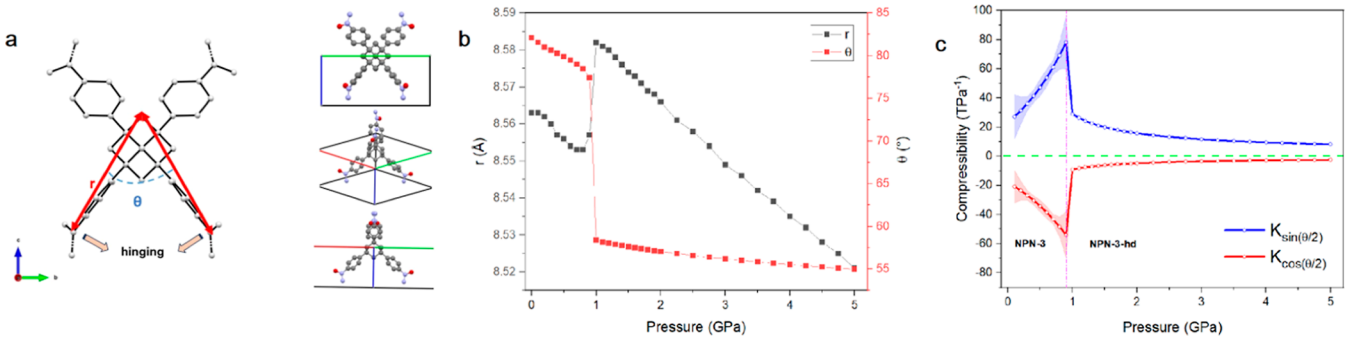

Figure 4. (a) Illustration of the strut (r) and hinge angle (θ) on the monomer. (b) Evolution of r and θ as a function of pressure. (c) Variations of compressibility for cos θ and sin θ.

and 7.6%, respectively. In the tensile region, the phase transition of NPN-3-hd is also an isosymmetric transition from cp-to-op. The metastable phase-IV has an SAV of about 36% and reverts to NPN-3 when the hydrostatic tensile pressure is released. To summarize, NPN-3 undergoes a series of structural transformations including op-to-cp and cp-to-op isosymmetric phase transitions in the hydrostatic compression and tensile regions, forming a hysteresis in the $P-V$ diagram. To date, the underlying mechanisms of isosymmetric phase transitions, such as charge transfer, high-spin to low-spin transition, interlayer sliding, coordination number change, hydrogen bond rearrangement in organic materials, and disruption or rotation of the octahedral sublattice, have been attributed to many materials.[58] However, in the case of NPN-3, the conformation of the monomer and the structural motif play a significant role in these transitions, which is further discussed.

Figure 2c,d illustrates the evolution of the cell parameters under hydrostatic pressure. It is evident that the *a*- and *b*-lattice parameters exhibit the same trend as the volume, contracting during compression and expanding during the cp-to-op phase transition of NPN-3-hd. Remarkably, the *c*-lattice parameter expands in the compression region, indicating the occurrence of NLC in the structure. To determine the linear, $K_L = -\frac{1}{L}\left(\frac{dL}{dP}\right)_T$, the computational data was fitted with a linear dependence in the compression region both before and after the phase transition. The calculated linear compressibility using Pascal program[59] along the *a* (or *b*) and *c* for NPN-3 are 59.27 and −42.04 TPa^{-1}, respectively. As for NPN-3-hd, these values for the *a*- (or *b*-) and *c*-axes are 15.18 and −2.36 TPa^{-1}, respectively. Clearly, NPN-3 and NPN-3-hd show NLC along the *c*-axis and PLC along the *ab*-plane (Figure 3a,b).

These extraordinary piezo-mechanical properties, characteristic of NPN-3, are attributable to the diamondoid (**dia**) topology, a common feature in flexible MOFs and COFs.[60] Additionally, the exceptional adaptability of the tetraphenyl adamantane monomer due to the high degree of freedom to various conformations under pressure plays a pivotal role in these mechanical behaviors.[61] To this end, to explore the effects of the structural motif on these properties, lattice parameters can be precisely defined by using a well-defined strut length (r) and hinge angle (θ) (Figure 4a). The derivations for these expressions are presented in detail in the Supporting Information

$$c = 1.1r\cos\left(\frac{\theta}{2}\right)$$
$$a = b = 2.82r\sin\left(\frac{\theta}{2}\right) \quad (1)$$

https://doi.org/10.1021/acs.jpcc.3c06949
J. Phys. Chem. C 2024, 128, 588−596

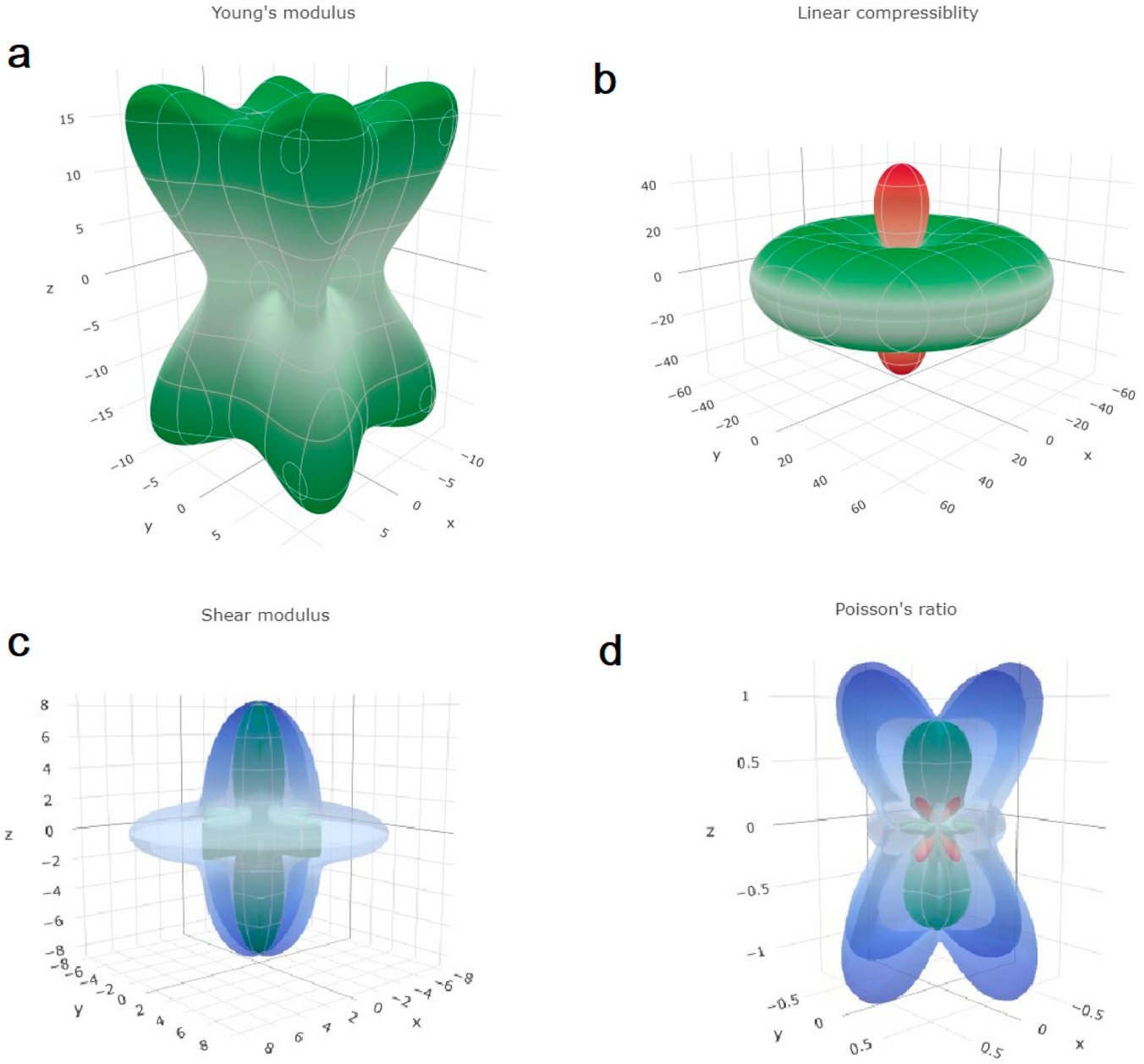

Figure 5. Three-dimensional representations of (a) Young's modulus, (b) linear compressibility, (c) shear modulus, and (d) Poisson's ratio. In (b), the green line represents PLC, while the red line denotes NLC, and the outer blue line signifies the maximum values, while the inner green line represents the minimum values. When considering spherical coordinates, the calculation of Poisson's ratio (ν) introduces an additional dimension, denoted by the angle χ, spanning from 0 to 2π. The blue region in (c) corresponds to the surface with the highest χ value, whereas the green (red) lobes indicate positive (negative) values of ν at the lowest χ value.

Variations in parameters r and θ under hydrostatic pressure are depicted in Figure 4b. Clearly, as pressure increases, the strut length decreases, and the hinge angle closes. The simultaneous decrease in both parameters results in a narrowing of the *ab*-plane, primarily due to the monomer extending diagonally across the *ab*-plane and an expansion of the *c*-axis (Figure 4a). A straightforward mathematical derivation enables us to express the linear compressibility of the unit cell parameters with respect to r and θ

$$K_c = K_r + K_{\cos(\theta/2)} \approx K_{\cos(\theta/2)} \qquad (K_r \approx 0)$$
$$K_a = K_r + K_{\sin(\theta/2)} \approx K_{\sin(\theta/2)} \qquad (K_r \approx 0) \qquad (2)$$

In the investigated pressure range, the change in the θ is notably more pronounced than that of the r, thus indicating that the structural response to pressure is primarily on θ. As depicted in Figure 4c, this trend in the hinge angle variation results in a negative $K_{\cos(\theta)}$ and a positive $K_{\sin(\theta)}$, aligning with the linear compressibility of the lattice parameters as shown in Figure 3a.

No significant elongation or shortening of the N═N and C−N bonds was observed, before and after the phase transitions. Similarly, the bond angles remain largely unchanged within the studied pressure range, preserving the near-perfect tetrahedral geometry of the monomer. These findings indicate that the subunit of NPN-3 maintains its structural integrity under pressure due to the presence of robust covalent bonds. However, compression did cause significant tilting of the nitrophenyl

https://doi.org/10.1021/acs.jpcc.3c06949
J. Phys. Chem. C 2024, 128, 588−596

groups. The degree of this tilting is determined by pressure-induced changes in the C−C−N−N and C−C−N−O dihedral angles. Due to the rotational flexibility of the C−N bond, it was observed that a tilting effect of up to 50% accommodated the compression, which also serves as the basis for the strut-hinge mechanism (Figure S3).

The underlying mechanism of the breathing effect behavior observed in NPN-3-hd can be also ascribed to the structural motif of the framework. In the tensile zone, which is in contrast to its behavior under compression, the structure elongates along the *a*/*b*-axes and contracts along the *c*-axis. As expected, the strut-hinge mechanism also operates in tension but in the opposite direction from its behavior under compression. Consequently, the rapid increase in the hinge angle of NPN-3-hd in the tensile region results in an isosymmetric phase transition, accompanied by a transition from a closed to an open pore structure (Figure S2). Apart from the structural motif, intermolecular interactions, notably hydrogen bonding, significantly impact both phase transitions and the mechanical properties of crystals. Indeed, C−H···O hydrogen bonds become dominant in the compression zone due to the proximity of nitroso and phenyl groups under pressure. Conversely, within the tensile region, the transition from NPN-3-hd to NPN-3 leads to a diminished dominance of C−H···O bonds due to the open pore structure. This observed alteration in C−H···O bonds under pressure within the investigated pressure range aligns with the *P*−*V* characteristics of the structure, suggesting a potential role for these bonds in the structural flexibility of NPN-3 (Figure S4).

The **dia** topology of the framework introduces anisotropy in its mechanical properties.[26] This directional dependence is evident in the 3D maps of elastic properties derived from elastic constants, as illustrated in Figure 5. Interestingly, the directions of coordination exhibit the highest mechanical strength, while the region along the center of the tetrahedral nodes represents the mechanically softest direction. The compressibility values computed from the elastic constants further confirm the existence of positive linear compressibility (PLC) along the *a*/*b*-axes and significant NLC along the *c*-axis. Similar to observations in other porous materials, the structure displays a minimum shear modulus within the *ab*-plane, coinciding with the location of open channels, and it exhibits the highest shear strength along the *c*-axis. Anisotropy is also apparent in Poisson's ratios, with the structure notably demonstrating negative Poisson's property along the *ac*-plane, suggesting its potential as an auxetic material.[62]

In practical terms, the search for materials that either have a large NLC value or exhibit an NLC effect over a wide pressure range is of great interest in this field. The ideal scenario would involve the discovery of materials that exhibit both properties simultaneously.[26] Figure 6 illustrates framework materials reported in the literature for their NLC properties. The majority of these reported structures exhibit NLC characteristics with values falling at or below 20 TPa^{-1}.[31,63−66] These materials, featuring relatively rigid structures, manifest NLC properties across a wide pressure region. The second group comprises structures displaying NLC values ranging from 20 to 30 TPa^{-1}, including MOFs from the MIL series known for their breathing effect properties.[27,28,35,67] Particularly noteworthy is the inclusion of NPN-3 among the structures displaying giant NLC—a term used to denote exceptionally potent NLC (K_{NLC} < −30 TPa^{-1}) that remain applicable over a range of industrially significant pressures, extending to at least 1 GPa.[22] Since the

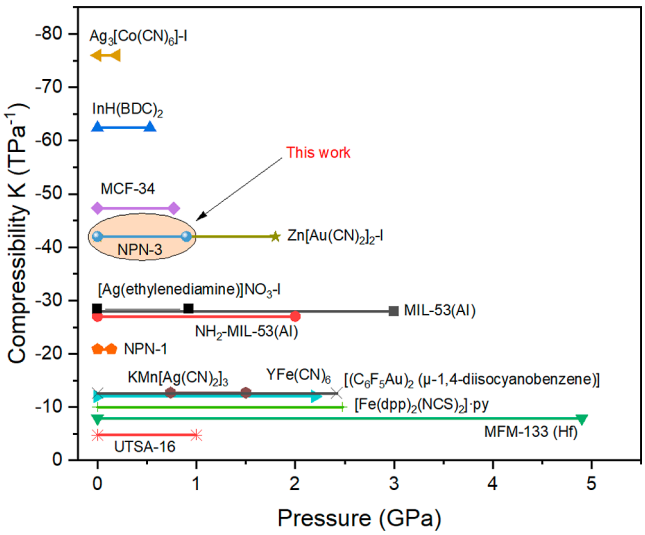

Figure 6. Reported framework materials showing the NLC effect. UTSA-16 (exp),[63] MFM-133 (Hf) (exp),[31] [$(C_6F_5Au)_2$(μ-1,4-diisocyanobenzene)] (exp),[64] [Fe(dpp)2(NCS)2]py (exp),[65] YFe-$(CN)_6$ (exp + DFT),[66] KMn[$Ag(CN)_2]_3$ (exp),[35] NPN-1 (DFT),[7] NH_2-MIL-53 (Al) (exp + DFT),[28] MIL-53(Al) (exp + DFT),[27] [Ag(ethylenediamine)]NO_3-I (exp),[67] Zn[$Au(CN)_2]_2$-I (exp),[22] MCF-34 (exp + DFT),[32] In$(BDC)_2$ (exp),[29] and Ag_3[$Co(CN)_6$]-I (exp).[21]

giant NLC phenomenon cannot be thermodynamically sustained indefinitely, the valid pressure range for such a phenomenon is quite narrow. All materials within this category undergo a phase transition subsequent to showing a giant NLC.[21,22,29,32] In instances where the structural motif is retained after the phase transition, the resulting material also exhibits NLC, albeit with a notable reduction due to the denser structure. NPN-3 exhibits all these typical features associated with materials displaying the giant NLC. Another significant finding is that NPN-1, previously reported as showing NLC, demonstrates valid NLC over a narrower pressure range compared to NPN-3. This difference can be attributed to the change of the tetrahedral node, from methane (as in NPN-1) to the more bulky adamantane (as in NPN-3), as well as a four- to six-fold increase in interpenetration along the *c*-axis within the structures.

CONCLUSIONS

In conclusion, in this comprehensive study, an anomalous set of piezo-mechanical properties of a 3D COF has been revealed by using DFT. Over a pressure range from −3 to 5 GPa, which encompasses tensile and compression regions, no amorphization or structural failure is experienced by the framework. This phenomenon is attributed to the strength of the covalent bonds, providing evidence that COFs are indeed mechanically more robust materials than MOFs. NPN-3 undergoes a pressure-induced first-order phase transition between 0.9 and 1 GPa. As a result of the isosymmetric phase transition, the NPN-3-hd phase, with the same crystal structure but higher density, is transformed into an actual closed pore form of NPN-3. Moreover, a giant NLC along the *c*-axis, a rarely observed phenomenon, is exhibited by NPN-3 prior to the phase transition. This unique NLC remains valid over a relatively wide pressure range, emphasizing its significance. More interestingly, while NPN-3 does not show any phase transition or anomaly in the tensile region, NPN-3-hd shows a phase

https://doi.org/10.1021/acs.jpcc.3c06949
J. Phys. Chem. C 2024, 128, 588−596

transition from a closed pore to an open pore, exhibiting the breathing-like effect previously reported for many MOFs. The origins of these remarkable piezo-mechanical properties lie in the diamondoid topology, which is a structural element commonly found in flexible MOFs and COFs. In addition, the extraordinary adaptability of the high degree of freedom of the tetraphenyl adamantane monomer to changing conformations under pressure plays a crucial role in these unique properties. It is proven in this study that the strut-hinge mechanism, which arises as a consequence of these two characters, is the origin of the indicated piezo-mechanical behaviors. These remarkable discoveries have profound implications for the utilization of COFs in piezo-mechanical sensors. The capability of NPN-3 to exhibit such prominent piezo-mechanical properties, including NLC and phase transitions, opens exciting possibilities for the development of advanced sensing technologies. Furthermore, the findings serve as an inspiring starting point for further research into the intricate mechanical behavior of COFs and their potential applications in new technologies.

■ ASSOCIATED CONTENT

Data Availability Statement

The data that support the findings of this study are available on request from the corresponding author.

Supporting Information

The Supporting Information is available free of charge at https://pubs.acs.org/doi/10.1021/acs.jpcc.3c06949.

Detailed description of the structural features of NPN-3 and NPN-3-hd (PDF)

■ AUTHOR INFORMATION

Corresponding Author

Mustafa Erkartal − *Department of Engineering Science, Abdullah Gul University, Kayseri 38080, Turkey;* orcid.org/0000-0002-9772-128X; Email: merkartal@mail.com, mustafa.erkartal@agu.edu.tr

Complete contact information is available at: https://pubs.acs.org/10.1021/acs.jpcc.3c06949

Notes

The author declares no competing financial interest.

■ ACKNOWLEDGMENTS

The calculations were run on The Scientific and Technological Research Council of Turkey (TÜBİTAK) ULAKBILIM-High Performance and Grid Computing Center (TRUBA) and AGU-HPC resources.

■ REFERENCES

(1) Schneemann, A.; Bon, V.; Schwedler, I.; Senkovska, I.; Kaskel, S.; Fischer, R. A. Flexible Metal-Organic Frameworks. *Chem. Soc. Rev.* **2014**, *43*, 6062−6096.

(2) Behera, N.; Duan, J. G.; Jin, W. Q.; Kitagawa, S. The Chemistry and Applications of Flexible Porous Coordination Polymers. *Energychem* **2021**, *3*, 100067.

(3) Seth, S.; Jhulki, S. Porous Flexible Frameworks: Origins of Flexibility and Applications. *Mater. Horiz.* **2021**, *8*, 700−727.

(4) Liu, Y.; Her, J. H.; Dailly, A.; Ramirez-Cuesta, A. J.; Neumann, D. A.; Brown, C. M. Reversible Structural Transition in Mil-53 with Large Temperature Hysteresis. *J. Am. Chem. Soc.* **2008**, *130*, 11813−11818.

(5) Yot, P. G.; Ma, Q.; Haines, J.; Yang, Q.; Ghoufi, A.; Devic, T.; Serre, C.; Dmitriev, V.; Férey, G.; Zhong, C.; et al. Large Breathing of the Mof Mil-47(V-Iv) under Mechanical Pressure: A Joint Experimental-Modelling Exploration. *Chem. Sci.* **2012**, *3*, 1100−1104.

(6) Kang, C.; Zhang, Z.; Kusaka, S.; Negita, K.; Usadi, A. K.; Calabro, D. C.; Baugh, L. S.; Wang, Y.; Zou, X.; Huang, Z.; et al. Covalent Organic Framework Atropisomers with Multiple Gas-Triggered Structural Flexibilities. *Nat. Mater.* **2023**, *22*, 636−643.

(7) Erkartal, M. Unveiling the Multifaceted Properties of a 3d Covalent-Organic Framework: Pressure-Induced Phase Transition, Negative Linear Compressibility and Auxeticity. *Comput. Mater. Sci.* **2023**, *227*, 112275.

(8) Georgieva, V. M.; Bruce, E. L.; Verbraeken, M. C.; Scott, A. R.; Casteel, W. J.; Brandani, S.; Wright, P. A. Triggered Gate Opening and Breathing Effects During Selective Co2 Adsorption by Merlinoite Zeolite. *J. Am. Chem. Soc.* **2019**, *141*, 12744−12759.

(9) Lozinska, M. M.; Mangano, E.; Greenaway, A. G.; Fletcher, R.; Thompson, S. P.; Murray, C. A.; Brandani, S.; Wright, P. A. Cation Control of Molecular Sieving by Flexible Li-Containing Zeolite Rho. *J. Phys. Chem. C* **2016**, *120*, 19652−19662.

(10) Peng, S. Q.; Yang, T. Y.; Fan, W. H.; Chi, S. M.; Kuang, B. Y.; Fan, L.; Li, X. D.; Huang, M. H. Flexible Porous Polynorbornenes with Alkene Linkage for Decolorizing the Highly Reactive Triisocyanate in Ethyl Acetate. *Chem. Mater.* **2022**, *34*, 5184−5193.

(11) Jin, F. Z.; Liu, J. J.; Chen, Y.; Zhang, Z. J. Tethering Flexible Polymers to Crystalline Porous Materials: A Win-Win Hybridization Approach. *Angew. Chem., Int. Ed.* **2021**, *60*, 14222−14235.

(12) Garai, B.; Bon, V.; Krause, S.; Schwotzer, F.; Gerlach, M.; Senkovska, I.; Kaskel, S. Tunable Flexibility and Porosity of the Metal-Organic Framework Dut-49 through Postsynthetic Metal Exchange. *Chem. Mater.* **2020**, *32*, 889−896.

(13) Wei, Y.-S.; Chen, K.-J.; Liao, P.-Q.; Zhu, B.-Y.; Lin, R.-B.; Zhou, H.-L.; Wang, B.-Y.; Xue, W.; Zhang, J.-P.; Chen, X.-M. Turning on the Flexibility of Isoreticular Porous Coordination Frameworks for Drastically Tunable Framework Breathing and Thermal Expansion. *Chem. Sci.* **2013**, *4*, 1539−1546.

(14) Agarwal, R. A.; Gupta, A. K.; De, D. Flexible Zn-MOF Exhibiting Selective CO_2 Adsorption and Efficient Lewis Acidic Catalytic Activity. *Cryst. Growth Des.* **2019**, *19*, 2010−2018.

(15) Chen, Y. W.; Idrees, K. B.; Son, F. A.; Wang, X. J.; Chen, Z. J.; Xia, Q. B.; Li, Z.; Zhang, X.; Farha, O. K. Tuning the Structural Flexibility for Multi-Responsive Gas Sorption in Isonicotinate-Based Metal-Organic Frameworks. *ACS Appl. Mater. Interfaces* **2021**, *13*, 16820−16827.

(16) Ernst, M.; Poręba, T.; Gnägi, L.; Gryn'ova, G. Locating Guest Molecules inside Metal-Organic Framework Pores with a Multilevel Computational Approach. *J. Phys. Chem. C* **2023**, *127*, 523−531.

(17) Wang, X. G.; Xu, L.; Li, M. J.; Zhang, X. Z. Construction of Flexible-on-Rigid Hybrid-Phase Metal-Organic Frameworks for Controllable Multi-Drug Delivery. *Angew. Chem., Int. Ed.* **2020**, *59*, 18078−18086.

(18) Dong, J. Q.; Wee, V.; Zhao, D. Stimuli-Responsive Metal-Organic Frameworks Enabled by Intrinsic Molecular Motion. *Nat. Mater.* **2022**, *21*, 1334−1340.

(19) Zhu, K.; Cao, Y.; Fan, R. Q.; Zhang, J.; Jia, W. W.; Jiang, X.; Ji, C. S.; Wu, J. K.; Yin, Y. Y.; Yang, Y. L. Stimuli-Responsive of Flexible Silver-Organic Framework Film with Molecular Rotors Based on Methylene Rotation. *Small Struct.* **2022**, *3*, 2200108.

(20) Coudert, F.-X.; Evans, J. D. Nanoscale Metamaterials: Meta-Mofs and Framework Materials with Anomalous Behavior. *Coord. Chem. Rev.* **2019**, *388*, 48−62.

(21) Goodwin, A. L.; Keen, D. A.; Tucker, M. G. Large negative linear compressibility of $Ag_3[Co(CN)_6]$. *Proc. Natl. Acad. Sci. U.S.A.* **2008**, *105*, 18708−18713.

(22) Cairns, A. B.; Catafesta, J.; Levelut, C.; Rouquette, J.; van der Lee, A.; Peters, L.; Thompson, A. L.; Dmitriev, V.; Haines, J.; Goodwin, A. L. Giant Negative Linear Compressibility in Zinc Dicyanoaurate. *Nat. Mater.* **2013**, *12*, 212−216.

(23) Qiu, W. B.; Zeng, Q. X.; Li, C. X.; Hao, J.; Li, Y. W. Theoretical Investigation of Zero Linear Compressibility on Metal Squarates MC_4O_4 (M = Pb and Ba). *J. Phys. Chem. C* **2023**, *127*, 9957−9963.

(24) Zeng, Q.; Qiu, W.; Hao, J.; Wang, K.; Li, Y. Tunable Zero Linear Compressibility under a Rational Designed Mechanism of Modular "Dumbbell": A Density Functional Theory Study. *ACS Mater. Lett.* **2022**, *4*, 541−547.
(25) Erkartal, M. Extreme Flexibility and Unusual Piezomechanical Properties of Zinc-Alkyl-Based Metal-Organic Frameworks: A First Principles Study. *Mater. Today Commun.* **2023**, *35*, 106054.
(26) Cairns, A. B.; Goodwin, A. L. Negative Linear Compressibility. *Phys. Chem. Chem. Phys.* **2015**, *17*, 20449−20465.
(27) Jiang, D. Q.; Wen, T.; Guo, Y. Z.; Liang, J.; Jiang, Z. M.; Li, C.; Liu, K.; Yang, W. G.; Wang, Y. G. Reentrant Negative Linear Compressibility in Mil-53(Al) over an Ultrawide Pressure Range. *Chem. Mater.* **2022**, *34*, 2764−2770.
(28) Serra-Crespo, P.; Dikhtiarenko, A.; Stavitski, E.; Juan-Alcañiz, J.; Kapteijn, F.; Coudert, F. X.; Gascon, J. Experimental Evidence of Negative Linear Compressibility in the Mil-53 Metal-Organic Framework Family. *CrystEngComm* **2015**, *17*, 276−280.
(29) Zeng, Q. X.; Wang, K.; Zou, B. Large Negative Linear Compressibility in $InH(BDC)_2$ from Framework Hinging. *J. Am. Chem. Soc.* **2017**, *139*, 15648−15651.
(30) Ortiz, A. U.; Boutin, A.; Gagnon, K. J.; Clearfield, A.; Coudert, F. X. Remarkable Pressure Responses of Metal-Organic Frameworks: Proton Transfer and Linker Coiling in Zinc Alkyl Gates. *J. Am. Chem. Soc.* **2014**, *136*, 11540−11545.
(31) Yan, Y.; O'Connor, A. E.; Kanthasamy, G.; Atkinson, G.; Allan, D. R.; Blake, A. J.; Schröder, M. Unusual and Tunable Negative Linear Compressibility in the Metal-Organic Framework Mfm-133(M) (M = Zr, Hf). *J. Am. Chem. Soc.* **2018**, *140*, 3952−3958.
(32) Zeng, Q. X.; Wang, K.; Zou, B. Negative Linear Compressibility Response to Pressure in Multitype Wine-Rack Metal-Organic Frameworks. *ACS Mater. Lett.* **2020**, *2*, 291−295.
(33) Zeng, Q. X.; Wang, K.; Qiao, Y. C.; Li, X. D.; Zou, B. Negative Linear Compressibility Due to Layer Sliding in a Layered Metal-Organic Framework. *J. Phys. Chem. Lett.* **2017**, *8*, 1436−1441.
(34) Sun, S. J.; Henke, S.; Wharmby, M. T.; Yeung, H. H. M.; Li, W.; Cheetham, A. K. Mechanical Properties of a Calcium Dietary Supplement, Calcium Fumarate Trihydrate. *Inorg. Chem.* **2015**, *54*, 11186−11192.
(35) Cairns, A. B.; Thompson, A. L.; Tucker, M. G.; Haines, J.; Goodwin, A. L. Rational Design of Materials with Extreme Negative Compressibility: Selective Soft-Mode Frustration in Kmn[Ag(Cn)]. *J. Am. Chem. Soc.* **2012**, *134*, 4454−4456.
(36) Colmenero, F.; Timón, V. Zif-75 under Pressure: Negative Linear Compressibility and Pressure-Induced Instability. *Appl. Sci.* **2022**, *12*, 10413.
(37) Li, H. Y.; Brédas, J. L. Impact of Structural Defects on the Elastic Properties of Two-Dimensional Covalent Organic Frameworks (2d Cofs) under Tensile Stress. *Chem. Mater.* **2021**, *33*, 4529−4540.
(38) Zhang, J. Phase Transformation in Two-Dimensional Covalent Organic Frameworks under Compressive Loading. *Phys. Chem. Chem. Phys.* **2018**, *20*, 29462−29471.
(39) Zhou, W.; Wu, H.; Yildirim, T. Structural Stability and Elastic Properties of Prototypical Covalent Organic Frameworks. *Chem. Phys. Lett.* **2010**, *499*, 103−107.
(40) Sun, J. H.; Iakunkov, A.; Baburin, I. A.; Joseph, B.; Palermo, V.; Talyzin, A. V. Covalent Organic Framework (Cof-1) under High Pressure. *Angew. Chem., Int. Ed.* **2020**, *59*, 1087−1092.
(41) Guan, X. Y.; Chen, F. Q.; Fang, Q. R.; Qiu, S. L. Design and Applications of Three Dimensional Covalent Organic Frameworks. *Chem. Soc. Rev.* **2020**, *49*, 1357−1384.
(42) Giannozzi, P.; Baroni, S.; Bonini, N.; Calandra, M.; Car, R.; Cavazzoni, C.; Ceresoli, D.; Chiarotti, G. L.; Cococcioni, M.; Dabo, I.; et al. Quantum Espresso: A Modular and Open-Source Software Project for Quantum Simulations of Materials. *J. Phys.: Condens.Matter* **2009**, *21*, 395502.
(43) Blöchl, P. E. Projector Augmented-Wave Method. *Phys. Rev. B: Condens. Matter Mater. Phys.* **1994**, *50*, 17953−17979.
(44) Ghosh, P. S.; Ponomareva, I. Negative Linear Compressibility in Organic-Inorganic Hybrid Perovskite [Nh2nh3]X(Hcoo)3 (X = Mn, Fe, Co). *J. Phys. Chem. Lett.* **2022**, *13*, 3143−3149.
(45) Ghosh, P. S.; Ponomareva, I. Negative Linear Compressibility in $[NH_3NH_2]Co(HCOO)_3$ and Its Structural Origin Revealed from First Principles. *J. Phys. Chem. Lett.* **2021**, *12*, 7560−7565.
(46) Perdew, J. P.; Burke, K.; Ernzerhof, M. Generalized Gradient Approximation Made Simple. *Phys. Rev. Lett.* **1996**, *77*, 3865−3868.
(47) Grimme, S. Semiempirical Gga-Type Density Functional Constructed with a Long-Range Dispersion Correction. *J. Comput. Chem.* **2006**, *27*, 1787−1799.
(48) Billeter, S. R.; Turner, A. J.; Thiel, W. Linear Scaling Geometry Optimisation and Transition State Search in Hybrid Delocalised Internal Coordinates. *Phys. Chem. Chem. Phys.* **2000**, *2*, 2177−2186.
(49) Monkhorst, H. J.; Pack, J. D. Special Points for Brillouin-Zone Integrations. *Phys. Rev. B: Solid State* **1976**, *13*, 5188−5192.
(50) Dal Corso, A. Elastic Constants of Beryllium: A First-Principles Investigation. *J. Phys.: Condens.Matter* **2016**, *28*, 075401.
(51) Spek, A. L. Single-crystal structure validation with the program*PLATON*. *J. Appl. Crystallogr.* **2003**, *36*, 7−13.
(52) Gaillac, R.; Pullumbi, P.; Coudert, F. X. Elate: An Open-Source Online Application for Analysis and Visualization of Elastic Tensors. *J. Phys.: Condens.Matter* **2016**, *28*, 275201.
(53) Hirel, P. Atomsk: A Tool for Manipulating and Converting Atomic Data Files. *Comput. Phys. Commun.* **2015**, *197*, 212−219.
(54) Beaudoin, D.; Maris, T.; Wuest, J. D. Constructing Monocrystalline Covalent Organic Networks by Polymerization. *Nat. Chem.* **2013**, *5*, 830−834.
(55) Clarke, S. M.; Steele, B. A.; Kroonblawd, M. P.; Zhang, D. Z.; Kuo, I. F. W.; Stavrou, E. An Isosymmetric High-Pressure Phase Transition in A-Glycylglycine: A Combined Experimental and Theoretical Study. *J. Phys. Chem. B* **2020**, *124*, 1−10.
(56) Ortiz, A. U.; Boutin, A.; Coudert, F. X. Prediction of Flexibility of Metal-Organic Frameworks Cau-13 and Nott-300 by First Principles Molecular Simulations. *Chem. Commun.* **2014**, *50*, 5867−5870.
(57) Alhamami, M.; Doan, H.; Cheng, C. H. A Review on Breathing Behaviors of Metal-Organic-Frameworks (Mofs) for Gas Adsorption. *Materials* **2014**, *7*, 3198−3250.
(58) Christy, A. G. Isosymmetric Structural Phase-Transitions - Phenomenology and Examples. *Acta Crystallogr., Sect. B: Struct. Sci., Cryst. Eng. Mater.* **1995**, *51*, 753−757.
(59) Cliffe, M. J.; Goodwin, A. L. *PASCal*: a principal axis strain calculator for thermal expansion and compressibility determination. *J. Appl. Crystallogr.* **2012**, *45*, 1321−1329.
(60) Borgmans, S.; Rogge, S. M. J.; De Vos, J. S.; Van Der Voort, P.; Van Speybroeck, V. Exploring the Phase Stability in Interpenetrated Diamondoid Covalent Organic Frameworks. *Commun. Chem.* **2023**, *6*, 5.
(61) Knop, O.; Rankin, K. N.; Cameron, T. S.; Boyd, R. J. Crystal chemistry of tetraradial species. Part 10. Tilting at windmills: conformations of the tetraphenyl species $ZPh_4^{0,\pm1}$ (Z = B, C, N). *Can. J. Chem.* **2002**, *80*, 1351−1366.
(62) Ryder, M. R.; Tan, J.-C. Explaining the Mechanical Mechanisms of Zeolitic Metal-Organic Frameworks: Revealing Auxeticity and Anomalous Elasticity. *Dalton Trans.* **2016**, *45*, 4154−4161.
(63) Binns, J.; Kamenev, K. V.; Marriott, K. E. R.; McIntyre, G. J.; Moggach, S. A.; Murrie, M.; Parsons, S. A Non-Topological Mechanism for Negative Linear Compressibility. *Chem. Commun.* **2016**, *52*, 7486−7489.
(64) Woodall, C. H.; Beavers, C. M.; Christensen, J.; Hatcher, L. E.; Intissar, M.; Parlett, A.; Teat, S. J.; Reber, C.; Raithby, P. R. Hingeless Negative Linear Compression in the Mechanochromic Gold Complex [(C6f5au)2(M-1,4-Diisocyanobenzene)]. *Angew. Chem., Int. Ed.* **2013**, *52*, 9691−9694.
(65) Shepherd, H. J.; Palamarciuc, T.; Rosa, P.; Guionneau, P.; Molnár, G.; Létard, J.; Bousseksou, A. Antagonism between Extreme Negative Linear Compression and Spin Crossover in $[Fe(dpp)_2(NCS)_2]\cdot py$. *Angew. Chem., Int. Ed.* **2012**, *51*, 3910−3914.

https://doi.org/10.1021/acs.jpcc.3c06949
J. Phys. Chem. C 2024, 128, 588−596

(66) Duyker, S. G.; Peterson, V. K.; Kearley, G. J.; Studer, A. J.; Kepert, C. J. Extreme Compressibility in Lnfe(Cn)6 Coordination Framework Materials Via Molecular Gears and Torsion Springs. *Nat. Chem.* **2016**, *8*, 270−275.
(67) Cai, W.; Katrusiak, A. Giant Negative Linear Compression Positively Coupled to Massive Thermal Expansion in a Metal-Organic Framework. *Nat. Commun.* **2014**, *5*, 4337.

https://doi.org/10.1021/acs.jpcc.3c06949
J. Phys. Chem. C 2024, 128, 588−596